Physica Medica 119 (2024) 103315

Contents lists available at ScienceDirect

Physica Medica

journal homepage: www.elsevier.com/locate/ejmp

Attention-based deep neural network for partial volume correction in brain ^{18}F-FDG PET imaging

MohammadSaber Azimi [a], Alireza Kamali-Asl [a,*], Mohammad-Reza Ay [b,c], Navid Zeraatkar [d], Mahboube-Sadat Hosseini [a], Amirhossein Sanaat [e], Hossein Arabi [e,*]

[a] Department of Medical Radiation Engineering, Shahid Beheshti University, Tehran, Iran
[b] Research Center for Molecular and Cellular Imaging (RCMCI), Advanced Medical Technologies and Equipment Institute (AMTEI), Tehran University of Medical Sciences (TUMS), Tehran, Iran
[c] Department of Medical Physics and Biomedical Engineering, Tehran University of Medical Sciences, Tehran, Iran
[d] Siemens Medical Solutions USA, Inc., Knoxville, TN, USA
[e] Division of Nuclear Medicine & Molecular Imaging, Geneva University Hospital, CH-1211 Geneva, Switzerland

ARTICLE INFO

Keywords:
PET
Partial volume effect
Deep learning
Attention-based

ABSTRACT

Purpose: This work set out to propose an attention-based deep neural network to predict partial volume corrected images from PET data not utilizing anatomical information.
Methods: An attention-based convolutional neural network (ATB-Net) is developed to predict PVE-corrected images in brain PET imaging by concentrating on anatomical areas of the brain. The performance of the deep neural network for performing PVC without using anatomical images was evaluated for two PVC methods, including iterative Yang (IY) and reblurred Van-Cittert (RVC) approaches. The RVC and IY PVC approaches were applied to PET images to generate the reference images. The training of the U-Net network for the partial volume correction was trained twice, once without using the attention module and once with the attention module concentrating on the anatomical brain regions.
Results: Regarding the peak signal-to-noise ratio (PSNR), structural similarity index (SSIM), and root mean square error (RMSE) metrics, the proposed ATB-Net outperformed the standard U-Net model (without attention compartment). For the RVC technique, the ATB-Net performed just marginally better than the U-Net; however, for the IY method, which is a region-wise method, the attention-based approach resulted in a substantial improvement. The mean absolute relative SUV difference and mean absolute relative bias improved by 38.02 % and 91.60 % for the RVC method and 77.47 % and 79.68 % for the IY method when using the ATB-Net model, respectively.
Conclusions: Our results propose that without using anatomical data, the attention-based DL model could perform PVC on PET images, which could be employed for PVC in PET imaging.

1. Introduction

The partial volume effect (PVE) can limit the accuracy of Positron Emission Tomography (PET) images, particularly for features that are similar in size to the spatial resolution of the system (or point spread function - PSF), leading to noticeable spill-in and spill-out across adjacent regions and resulting in obvious biases [1–3]. Prior to the measurement of lesion/organ metabolism and physiology, partial volume correction (PVC) may be necessary to take into account signal alteration due to the limited spatial resolution of the PET system. Many PVC approaches require an accurate definition of the anatomical boundaries, which necessitate concurrent anatomical imaging such as MRI. CT images do not provide detailed anatomical information of the brain structure, unlike MR images. While major tissue structures, such as soft tissue, bone, and air, can be easily distinguished in CT images, they do not provide anatomical details of the brain [4–6]. The utilization of anatomical information may not be possible due to the patient's uncontrolled movements during image acquisition and mismatches between anatomical and functional data [1,7–9]. Deep learning (DL) approaches have already been utilized to perform PVC for PET images with and without employing anatomical information [10–14].

In conventional deep learning training, the collection of reference

* Corresponding authors.
E-mail addresses: A_r_kamali@yahoo.com (A. Kamali-Asl), hossein.arabi@unige.ch (H. Arabi).

https://doi.org/10.1016/j.ejmp.2024.103315
Received 25 January 2023; Received in revised form 4 October 2023; Accepted 5 February 2024
Available online 19 February 2024
1120-1797/© 2024 Associazione Italiana di Fisica Medica e Sanitaria. Published by Elsevier Ltd. All rights reserved.

datasets is critical; however, acquiring an underlying radiotracer uptake map in the brain is not practically feasible. To address this challenge, simulation data and/or synthetic data generated by the cycle generative adversarial network (CycleGAN) can be exploited to develop deep learning models [15–17]. Nevertheless, the simulation and synthetic data may not be realistic enough to develop a robust deep learning-based model. In this light, partial volume corrected PET data using anatomical MR data and/or brain templates are regarded as a reference for developing deep learning models [11].

In our previous works [10–12], the performance of deep neural networks to perform PVC without using anatomical images was assessed for six different PVC methods, including geometric transfer matrix (GTM) [4], multi-target correction (MTC) [18], region-based voxel-wise correction (RBV) [19], iterative Yang (IY) [20], reblurred Van-Cittert (RVC) [5], and Richardson-Lucy (RL) [5]. Different levels of error were observed for the different PVC methods. This is due to the fact that DL methods generally process the whole input image, while some PVC methods, such as GTM, rely on user-defined volumes of interest (VOIs) or anatomical regions (in the form of binary masks for the different brain regions) for the estimation of PVE-corrected activity concentrations.

Attention-based neural networks have been proposed as a way to improve the performance of deep learning algorithms. These networks work by creating an attention map that identifies the most important parts of the input image dataset for the given task. By doing so, the network is able to extract meaningful and discriminative features from these key regions while disregarding less important ones. This approach helps to improve the overall performance of the network [19,21,22].

Since PVC entails a particular focus on the boundaries of the anatomical regions, an attention-based deep learning solution would be efficient for this task. In this regard, an attention-based convolutional neural network (ATB-Net) was proposed to conduct PVC on brain PET images. The objective was to build a model that could generate partial volume corrected images from PET images while concentrating on the critical brain areas. Therefore, the model explicitly targets anatomical brain regions and does not consider areas such as the neck and tumor regions. To this end, a modified encoder-decoder U-Net [23,24] with an extra compartment was designed to focus on the anatomical areas of the brain, converting the Automated Anatomical Labeling (AAL)[19] brain map into an attention map. To our knowledge, this is the first time an attention-based convolutional neural network has been employed to perform PVC on PET scans. Two PVC techniques, IY and RVC [5,20], were employed to examine the performance of the proposed ATB-Net. In addition, a conventional U-Net model was trained to investigate the effect of the attention compartment in the ATB-Net model on the predicted partial volume corrected images.

2. Materials and methods

2.1. Data acquisition

In this study, a total of 160 patients diagnosed with head and neck tumors were enrolled. The patient data was randomly divided into three datasets, with 100 patients for training, 20 for validation, and 40 for external testing. It is important to note that only patients with head cancer were included in this study to evaluate their brain area. Written consent was acquired from patients who participated in this study. Following injection of a typical ^{18}F-FDG dosage of 205 ± 10 MBq, all patients were scanned on a PET/CT scanner (Biograph 16 PET/CT scanner, Siemens Healthineers, Germany). The intensity values of the PET images were converted into Standardized Uptake Values (SUV), and the PET images were resampled to an isotropic voxel size of (2 mm)^3. The PET images were then cropped into a matrix size of 144 × 144 × 120 so that the data was explicitly focused on the brain to remove the irrelevant surrounding air and neck before the development of the deep learning networks. Detailed demographic information of the patients is summarized in Table 1.

Table 1
Demographics of patients included in this study.

	Training	Test	Validation
Number	100	40	20
Male/Female	59/41	23/17	12/8
Age (mean ± SD)	63 ± 8	60 ± 18	63 ± 4.5
Weight (Mean ± SD)	71 ± 6	69 ± 12	72 ± 11
Indication/diagnosis	head and neck cancer staging or follow-up examinations		

2.2. Partial volume correction

The PETPVC toolbox [5,25], developed in C++ utilizing the insight segmentation and registration toolkit, included eight major post-reconstruction PVC algorithms and was employed to conduct PVC on PET images. To correct PET images for PVE, two commonly used PVC techniques, IY and RVC, were implemented. These two methods are elaborated in sections B.1 and B.2 in the following. Since the IY PVC approach is a region-based method, it requires anatomical masks of brain regions in order to estimate the activity concentration within each region. To obtain the anatomical brain regions, AAL brain atlas was co-registered to the PET data using AAL brain region transforms in MNI152 non-linear warp into the subject-space with the FSL tool. Providing a mask along with the co-registered AAL atlas to Atlasquery allows us to analyze specific regions of interest within the PET data and obtain information about those regions' anatomical labels and characteristics. By inputting the PET data and either the coordinates of interest or a mask, Atlasquery calculates and provides the average probability of the voxel or mask belonging to different labeled regions in the AAL atlas. When a mask is applied, the average probability is determined by considering all the voxels within the mask.

On the other hand, the RVC method is a deconvolution-based technique that does not require the anatomical mask. This method used the scanner's PSF to execute PVC through a deconvolution process. The study used a Biograph scanner (Siemens Healthineers), whose resolution is modeled as a PSF equivalent to a Gaussian function with Full-Width at Half-Maximum (FWHM) of 4–5 mm. A Gaussian kernel with the same FWHM was used to reconstruct the PET images in a shift-invariant manner. In this case, the RVC technique was fed with the PSF of the Biograph 16 scanner with a FWHM of 5 mm to conduct PVC.

2.2.1. Iterative Yang (IY)

The IY method [18], which is an improved version of the Yang method [19,26], relies on region of interests/anatomical masks to estimate mean value within each region from input PET data using Eq. (1):

$$f_{k+1}(x) = f(x)\left[\frac{s_k(x)}{s_k(x) \otimes h(x)}\right] \tag{1}$$

Here, $s_k(x) = \sum_{i=1}^{n}\left[T_{k,i}P_i(x)\right]$ is a piece-wise version of the PET image (based on the anatomical regions) with a mean value for each area, $T_{k,i}$ is the estimated mean value of region i at iteration k, h denotes the system's PSF, f is the input image, and f_k is the estimate of the partial volume corrected image at iteration k. According to Erlandsson et al. [27], the IY technique requires only 3–5 iterations. Therefore, 5 iterations were executed.

2.2.2. Deconvolution techniques (RVC)

Deconvolution-based approaches, which do not need anatomical knowledge or segmentation, were developed to correct for the PVE and blurring owing to the limited spatial resolution when high-resolution anatomical images are unavailable. The accuracy of these techniques is limited when the signal-to-noise ratio in the input images is not sufficiently high, which may result in noise amplification. Nevertheless, this approach could improve the image's contrast when no anatomical information is provided.

The RVC is implemented in an iterative fashion using Eq. (2) [19,28]:

$$f_{k+1}(x) = f_k(x) + \alpha . h(x) \otimes [f(x) - h(x) \otimes f_k(x)] \quad (2)$$

Here, α is the converging rate parameter which defines the level of correction at each iteration.

2.3. Deep neural network implementation

The architecture of the proposed ATB-Net is depicted in Fig. 1. This model comprises a modified U-shape encoder-decoder structure that takes PET images as input, wherein an extra compartment (attention module) creates the attention maps using the AAL brain map to define the anatomical regions. Through element-wise additions, the attention map is merged with the first layer of the main path, and the output of the combined layer is then transferred through the next layer of the main path. The modified U-Net is a fully convolutional network with deep concatenation connections between the corresponding stages in the encoder-decoder structure. Convolutional layers with 3 × 3 kernels and a rectified linear unit (ReLU) are employed at each level. A 22 % max-pooling is used to down-sample and up-sample data across the different stages. The Adam optimizer with a learning rate of 0.003 was used to train the network. The main goal was to train two independent DL models to synthesize the PVC images (one for IY and one for the RVC algorithm) from non-PVC PET images. In comparison to the U-Net network, the ATB-Net model benefits from a modified encoder-decoder structure and an extra compartment that generates the attention maps. The training of the ATB-Net and U-Net models was performed using 2D PET images (each transaxial slice as a single data sample), and overall, 4 PVC models were developed for the two PVC algorithms using the two deep learning models.

2.4. Performance evaluation

Standard quantitative measures, including the root mean square error (RMSE), peak signal-to-noise ratio (PSNR), structural similarity index metric (SSIM), Mean absolute relative bias (MARB), and mean absolute relative SUV difference (MARSUVD), were calculated between the reference and predicted PVC images by the U-Net and ATB-Net models to assess the performance of deep learning PVC solutions.

In addition to the SSIM, RMSE, and PSNR metrics, region-wise RMSE was calculated for the 71 anatomical brain regions defined by the AAL brain atlas. The symmetric regions in the left and right brain lobes were combined in the analyses to create 34 regions. Finally, using paired *t*-test analysis, the statistical significance of the differences between the U-Net and ATB-Net data was determined. A p-value less than 0.05 was considered as a statistically significant difference.

3. Results

Fig. 2 shows transaxial views of a sample input PET image (first row), reference PVE corrected PET images for IY and RVC approaches (second row), predicted PVE corrected images by the U-Net model (third row),

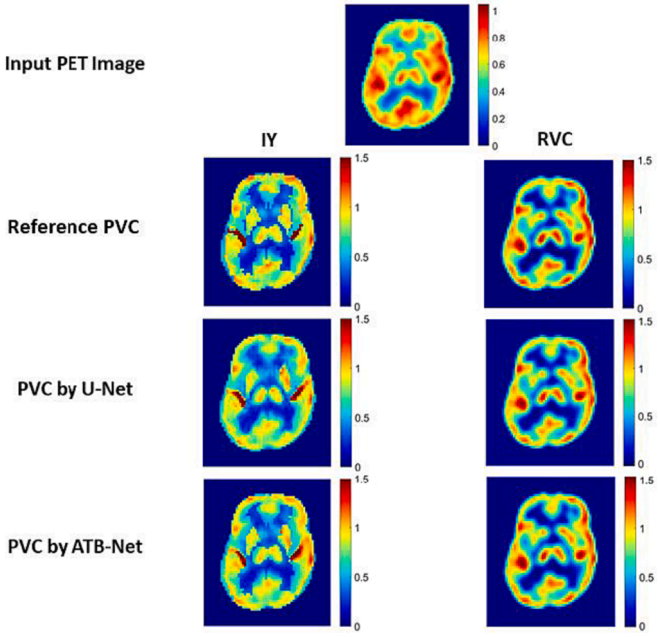

Fig. 2. Transaxial views of a representative PET image before PVC (first row), reference PVC PET images generated by the two PVC methods (second row), PVC PET images predicted by the U-Net model (third row), and PVC PET images predicted by the ATB-Net model for IY and RVC PVC approaches (forth row). These subjects from the test dataset have been diagnosed with brain and head tumors, but the brain images do not indicate any tumors or abnormalities.

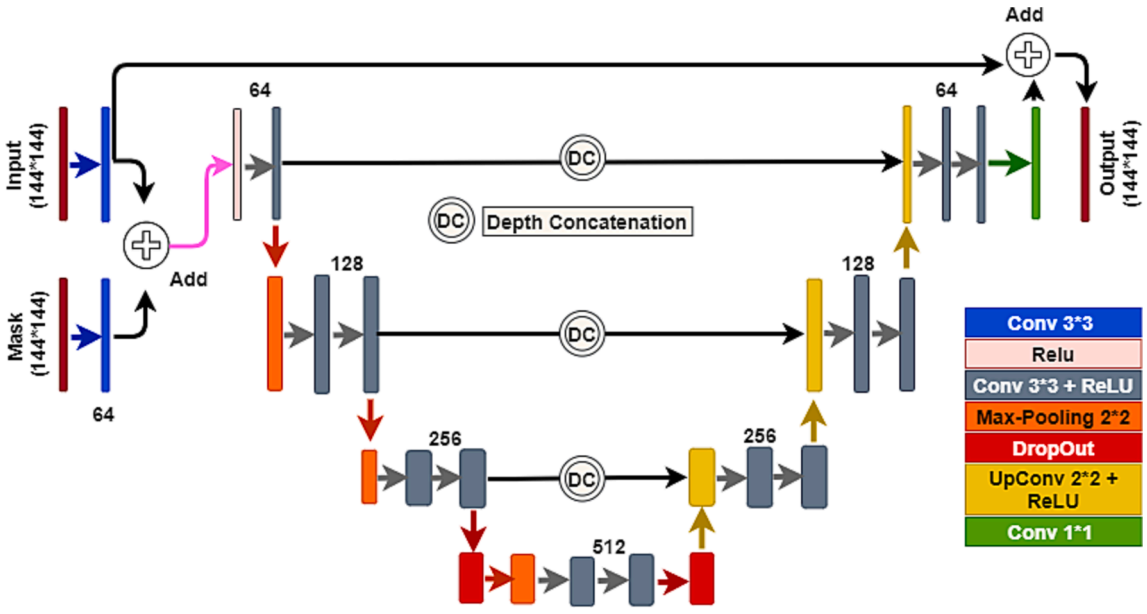

Fig. 1. Architecture of the proposed ATB-Net for predicting partial volume corrected images from PET images.

and predicted PVE corrected images by the proposed ATB-Net models for the two PVC algorithms (fourth row). The images predicted by the U-Net and the ATB-Net exhibit highly comparable structures/details to the reference PVC images regarding the visual assessment. On the other hand, IY images generated by the ATB-Net model contain sharp edges comparable to reference images, while IY images predicted by the U-Net model exhibited smoother structures/edges.

Table 2 and Fig. 3 summarize the findings of the quantitative assessments of the deep learning-based PVC models in terms of PSNR, RMSE, SSIM, MARSUVD, and MARB metrics for the U-Net and ATB-Net predicted images within the whole brain area.

The proposed ATB-Net model with PSNR of 27.20 and 22.64 and SSIM of 0.95 and 0.83 exhibited superior performance to the U-Net model with PSNR of 25.23 and 14.77 and SSIM of 0.94 and 0.67 for the RVC and IY approaches, respectively. Moreover, the ATB-Net model led to smaller RMSEs of 0.69 and 0.90 (in terms of SUV) for the RVC and IY approaches, respectively, compared to the U-Net model with RMSEs of 0.79 and 1.35. The boxplot of PSNR, RMSE, and SSIM results, as reported in Table 2, are presented in Fig. 3, while the bar plots of region-wises MARSUVD and MARB are shown in the Supplementary material.

Both the RVC and IY methods for the ATB-Net model outperformed their U-Net counterparts in terms of MARSUVD and MARB parameters. The values obtained for RVC were 0.12 and 1.25, while for IY, they were 0.41 and 4.46 respectively. These results highlight the superior performance of the ATB-Net model over the U-Net model in predicting both absolute SUV difference and absolute relative bias. The ATB-Net model has a lower network error rate and provides more accurate predictions of relative SUV difference compared to the U-Net model. The lower MARSUVD values indicate that the ATB-Net model produces more reliable predictions of relative SUV values with a reduced error rate.

Overall, the proposed ATB-Net outperformed the U-Net model in terms of MARB and MRSUVD by 91.60 %, 38.02 %, and 79.68 %, 77.47 %, for RVC and IY approaches, respectively. The PSNR, RMSE, SSIM, MARSUVD, and MARB values obtained from the U-Net and the proposed ATB-Net for the IY method showed statistically significant differences ($p < 0.05$). On the other hand, for the RVC method, only the MARSUVD and MARB values showed statistically significant differences between the U-Net and ATB-Net.

The summary of the region-wise (i.e., for the different anatomical brain regions) analysis of the two DL-based PVC models is presented in Figs. 4 and 5. The AAL brain atlas was used to identify 71 brain areas, and the region-wise RMSEs were calculated. The left and right symmetric regions were combined to reduce the number of brain areas to 34. Except for the Rolandic-Opcr, Supp-Motor-Area, Olfactory, Insula, Cingulum-Ant, Cingulum-Post, Hippo-Parahippo, Caudate Nucl, Heschl, and Vermis regions, the differences between the RMSEs obtained from the U-Net and the proposed ATB-Net model for the IY method were all statistically significant ($p < 0.05$). However, the RMSEs obtained from the proposed ATB-Net model and the U-Net for the RVC approach (Fig. 5) were all small.

Table 2
PSNR, RMSE and SSIM mean values and standard deviation calculated within the whole brain region for the PVC predicted images by U-Net and the proposed ATB-Net (separately for the RVC and IY approaches). The p-values have been calculated between the U-Net and ATB-Net for two IY and RVC models.

Test dataset	U-Net vs RVC	U-Net vs IY	ATB-Net vs RVC	ATB-Net vs IY	P value for RVC	P value for IY
PSNR	25.23 ± 5.71	14.77 ± 3.28	27.20 ± 4.78	22.64 ± 3.94	0.09	<0.01
RMSE (SUV)	0.79 ± 0.48	1.35 ± 0.48	0.69 ± 0.35	0.90 ± 0.39	0.26	<0.01
SSIM	0.94 ± 0.05	0.67 ± 0.06	0.95 ± 0.03	0.83 ± 0.04	0.11	<0.01
MARSUVD	1.24 ± 0.54	1.82 ± 0.75	0.12 ± 0.14	0.41 ± 0.22	<0.01	<0.01
MARB	14.99 ± 1.17	22.02 ± 1.68	1.25 ± 0.97	4.46 ± 1.88	<0.01	<0.01

4. Discussion

An attention-based deep learning model was implemented without utilizing anatomical images for PVC in PET imaging. Regarding the limited access to simultaneously acquired MR images, the proposed deep learning model performs PVC without using MR anatomical images. To accurately define the anatomical regions of the brain, the AAL brain map was employed, wherein an encoder-decoder U-Net with an extra compartment was designed, which translates the AAL brain map into an attention map. The reference images were created using two commonly used PVC methods, including the IY and RVC methods [5,19,20]. Visual assessment and quantitative evaluation demonstrated the ATB-Net model's promising performance for predicting the partial volume corrected PET images without using anatomical images, especially for the IY PVC method.

The ATB-Net network outperformed the U-Net model owing to the attention module, which concentrates on the key anatomical regions defined by the AAL template. The performance of deconvolution techniques such as RVC is limited (compared to the methods that employ anatomical images such as the IY approach) since these approaches rely solely on deconvolution processes to model/compensate for the spatial resolution of the PET system. When no anatomical information or proper segmentation is available, these approaches could offer at least a sub-optimal partial volume correction.

Table 3 displays the mean values of three parameters, RMSE, PSNR, and SSIM, obtained from the testing data of reference PVC images derived from IY and RVC methods.

Based on the comparison of PSNR, RMSE, and SSIM values in Table 2 with those in Table 3, it is evident that applying PVC to standard-dose PET images resulted in significant errors that led to reductions in SSIM, PSNR, and RMSE scores. This indicates that the PVC process introduced inaccuracies and inconsistencies in the images. However, both the U-Net and ATB-Net models were able to predict PVC images accurately. This suggests that these deep learning models were able to compensate for the errors introduced during the PVC process effectively. The U-Net model had higher MARSUVD values, indicating larger average differences between predicted and reference SUV values, whereas the ATB-Net model achieved lower MARSUVD values, indicating smaller average differences.

The results demonstrate that deep learning techniques are highly effective in enhancing PVC images. By reducing errors and improving accuracy, models such as U-Net and ATB-Net prove to be valuable tools in enhancing the quality and reliability of PVC images.

After examining and analyzing five different parameters – PSNR, RMSE, SSIM, MARB, and MARSUVD - for the results obtained from the ATB-Net and U-Net networks for two RVC and IY methods, it can be concluded that these networks were well investigated and analyzed. The performance of these methods was sufficient and satisfactory as deep learning was able to qualitatively and quantitatively improve the quality of PVC images in all parameters. Both models showed accurate predictions of PVC images, indicating that they effectively eliminated the errors introduced and compensated for the length of the PVC process. Furthermore, the ATB-Net network improved the quality of images and provided more reliable and accurate predictions.

For partial volume correction, Yuanyuan Gao et al. [29] investigated a voxel-based PVC approach using anatomical non-local means (NLMA) regularization and a least squares framework (LS). The well-known non-local means (NLM) filter takes advantage of the existing information redundancy within images to reduce image noise directly by replacing each voxel intensity with a weighted average of its non-local neighbors [30,31]. To conduct PVC, they considered NLM as a regularization term within an iterative-deconvolution model. In addition, an anatomically guided version of NLM was presented, which included MRI data into

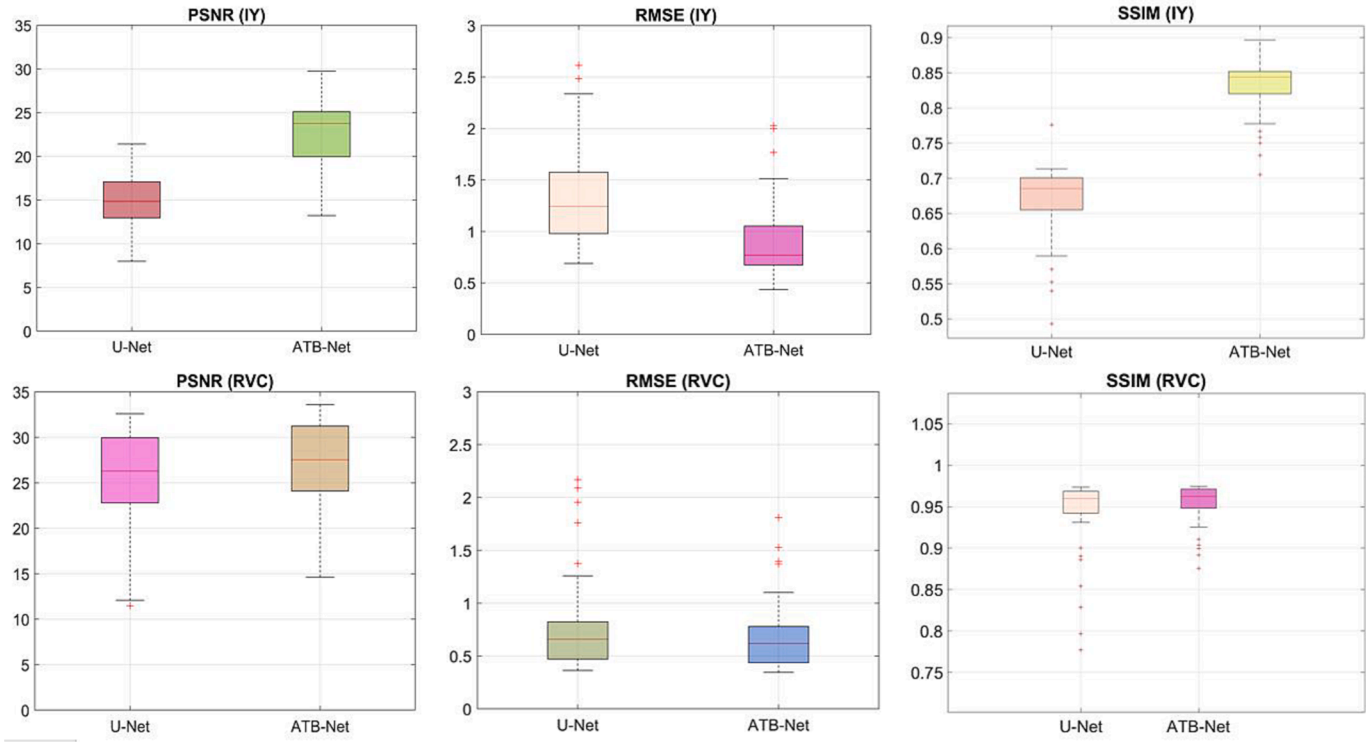

Fig. 3. Box plots of image quality metrics calculated for the U-Net and ATB-Net models over the entire brain region. First row) IY PVC method and second row) RVC PVC method.

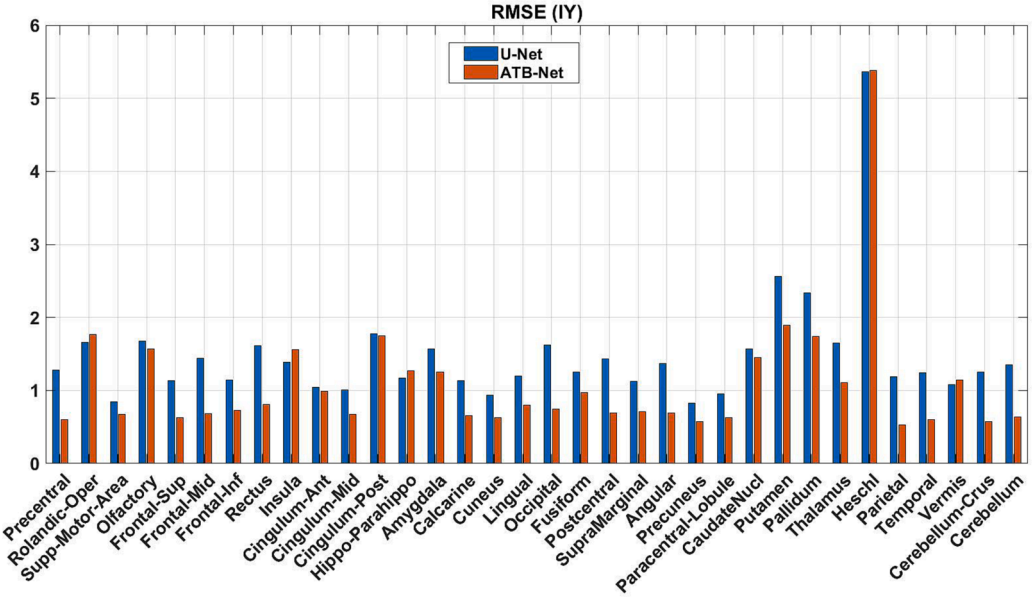

Fig. 4. Region-wise RMSEs obtained from the U-Net and ATB-Net models for the IY PVC method in 34 brain regions.

NLM to improve spatial resolution and reduce image noise. As a result, they showed that NLMA gives a better bias-noise trade-off compared to other PVC methods.

Chen et al. [32] exploited deep learning (DL) techniques to develop PVC for PET images using prior knowledge extracted from MR images. The development of deep learning models largely depends on reference data; however, the reference of the underlying anatomy and radiotracer uptake is inaccessible in clinical studies. In order to address this issue, a model trained on simulated data is transferred, which has easier access to reference. In this regard, PVC for PET images can be performed using a cycle-GAN model trained on simulated PET images. The developed deep learning model could be further fine-tuned to the clinical studies using transfer learning. The present work aimed to offer PVC solutions without requiring anatomical MR; however, the proposed model by Chen *et al.* [32] requires co-registered MR and PET data. Though incorporating anatomical MR images would enhance the performance of the deep learning model, this work aimed to develop an MR-independent PVC model wherein the attention module and the AAL brain map were employed to compensate for the lack of anatomical MR images.

Although the proposed ATB-Net exhibited only slightly better

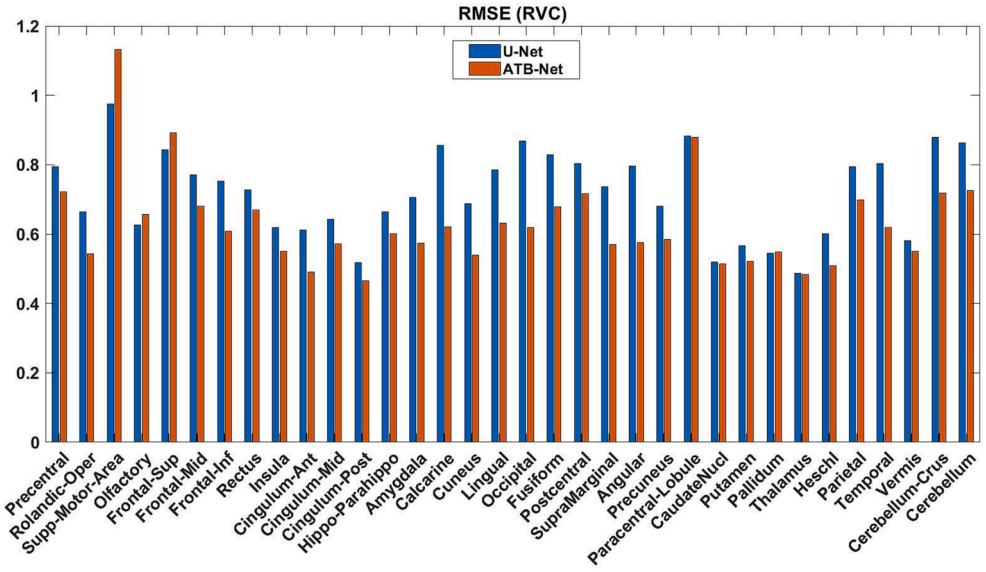

Fig. 5. Region-wise RMSEs obtained from the U-Net and ATB-Net models for the RVC method in 34 brain regions.

Table 3
Reference PVC images for the entire head region were used to calculate quantitative image quality metrics (mean ± SD).

Test dataset	RVC	IY
PSNR	18.07 ± 1.91	13.31 ± 2.49
RMSE (SUV)	2.87 ± 0.75	4.29 ± 1.47
SSIM	0.43 ± 0.05	0.36 ± 0.05

performance compared to the U-Net for the RVC method, superior performance was observed for the IY method when using the ATB-Net due to the fact that the IY method is a region-based method and the use of attention module and brain template aided to accurately predict the PVC PET images. IY approaches, correcting the entire image voxel by voxel, do not require any prior knowledge of the activity distribution and could be utilized for any number of areas. The RVC approach, on the other hand, is based on an additive correction step and assumes a Gaussian noise model. Due to noise amplification issues, RVC should be stopped after certain iterations, which may not reach its full convergence. However, one of the advantages of RVC over inverse filter (modeling the PSF of the system) is the ability to stop iterations before the artifacts appear. A duplicate of the original PET image is smoothed using a Gaussian-shaped kernel that represents the scanner's PSF in the RVC technique. Then, a different image is created between the smoothed version and the original PET image, which is added to the original unsmoothed PET image to produce a crisper image. This method is continued until a PET image with a significant improvement/modification is acquired after each cycle. The procedure will be discontinued when no improvement is observed as the iterations proceed. On the other hand, Iterative deconvolution enhances noise at each repetitive step, and the process is frequently terminated prematurely to prevent a low signal-to-noise ratio.

It is important to note that the quality of a PET scan image depends on the scanner's sensitivity and the imaging protocol used. The injection dose and scanning time may vary across different medical centers, however they are similar to a large extent. This would challenge the distribution of the proposed PVC method. Therefore, it is possible to employ transfer learning techniques using a small dataset from the target center or fine-tuning the model to new data to achieve optimal performance.

This study is limited in the sense that the partial volume effect was not corrected using patient-specific anatomical MR data, and instead, the AAL brain map was employed to implement PVC algorithms. In addition, since there were no ground-truth data (such as simulations) with which to compare the performance of the PVC algorithms, comparisons of the PVC algorithms were not possible. Thus, some of these algorithms may be intrinsically flawed, resulting in a negative impact on the deep learning models developed on their basis. To this purpose, certain common methodologies, such as the unrolling technique [33], should be adopted so that we can determine whether the inaccuracy is due to the PVC algorithm's suboptimal performance or poor deep learning training.

5. Conclusion

The attention-based deep learning model was shown to be capable of performing PVC methods on PET scans without the use of anatomical images to determine brain regions. When no MR images are available, the proposed attention-based deep learning model could be employed for PVC on PET-CT and/or PET-only images. We aim to expand the study by using inter-hospital patient data to remove potential bias in the trained network and make it more generalizable with more data for test. For the future, we suggest an unrolling algorithm to predict PV-corrected maps from PET images directly. Additionally, the techniques employed in this study can be applied to other body areas for a comprehensive understanding. Using an atlas for specific areas can streamline the process and ensure consistent results across studies.

CRediT authorship contribution statement

MS Azimi: Conceptualization, Data curation, Writing-original draft, Writing-review and editing, Visualization, Validation, Formal analysis, Methodology, Project administration, Software. **A Kamali-Asl:** Funding acquisition, Writing-review and editing, Investigation, Validation, Formal analysis, Supervision, Resources. **MR Ay:** Writing-review and editing, Investigation, Validation, Formal analysis, Supervision. **N Zeraatkar:** Conceptualization, Writing-review and editing, Formal analysis. **MS Hosseini:** Writing-original draft, Writing-review and editing, Visualization, Formal analysis, Methodology. **A Sanaat:** Conceptualization, Writing-review and editing. **H Arabi:** Data curation, Writing-original draft, Writing-review and editing, Investigation, Validation, Formal analysis, Supervision, Resources, Project administration, Software.

Declaration of competing interest

Dr. Zeraatkar is a full-time employee of Siemens Medical Solution, Inc., USA.

Acknowledgment

We want to express our sincere appreciation to our coworkers for their work on this project, especially Dr. Arman Rahmim for their invaluable technical assistance.

Ethical approval and consent to participate.

Written consents were acquired from participated patients, and the study was approved by the local ethic committee.

Consent for publication

All authors discussed and approved the final manuscript for submission.

References

[1] Boussion N, Le Rest CC, Hatt M, Visvikis D. Incorporation of wavelet-based denoising in iterative deconvolution for partial volume correction in whole-body PET imaging. Eur J Nucl Med Mol Imaging 2009;36(7):1064–75.
[2] Arabi H, Asl ARK. Feasibility study of a new approach for reducing of partial volume averaging artifact in CT scanner, in 2010 17th Iranian Conference of Biomedical Engineering (ICBME), 2010: IEEE, pp. 1-4.
[3] Belzunce MA, Mehranian A, Reader AJ. Enhancement of partial volume Correction in MR-guided PET image reconstruction by using MRI Voxel Sizes (in eng). IEEE Trans Radiat Plasma Med Sci May 2019;3(3):315–26. https://doi.org/10.1109/trpms.2018.2881248.
[4] Rousset OG, Ma Y, Evans AC. Correction for partial volume effects in PET: principle and validation. J Nucl Med 1998;39(5):904–11.
[5] Tohka J, Reilhac A. Deconvolution-based partial volume correction in Raclopride-PET and Monte Carlo comparison to MR-based method. Neuroimage 2008;39(4):1570–84.
[6] Erlandsson K, Dickson J, Arridge S, Atkinson D, Ourselin S, Hutton BF. MR imaging-guided partial volume correction of PET data in PET/MR imaging (in eng). PET Clin Apr 2016;11(2):161–77. https://doi.org/10.1016/j.cpet.2015.09.002.
[7] Soret M, Bacharach SL, Buvat I. Partial-volume effect in PET tumor imaging. J Nucl Med 2007;48(6):932–45.
[8] Boussion N, Hatt M, Reilhac A, Visvikis D. Fully automated partial volume correction in PET based on a wavelet approach without the use of anatomical information. In: *2007 IEEE Nuclear Science Symposium Conference Record*, vol. 4. IEEE; 2007. p. 2812–6.
[9] Arabi H, Zaidi H. MRI-guided attenuation correction in torso PET/MRI: Assessment of segmentation-, atlas-, and deep learning-based approaches in the presence of outliers (in eng). Magn Reson Med Feb 2022;87(2):686–701. https://doi.org/10.1002/mrm.29003.
[10] M.-S. Azimi, A. Kamali-Asl, M.-R. Ay, H. Arabi, and H. Zaidi, "A Novel Attention-based Convolutional Neural Network for Joint Denoising and Partial Volume Correction of Low-dose PET Images," presented at the 2021 IEEE Nuclear Science Symposium, Medical Imaging Conference and Room Temperature Semiconductor Detector Conference, Japan, 2021.
[11] M.-S. Azimi, A. Kamali-Asl, M.-R. Ay, N. Zeraatkar, and H. Arabi, "Deep Learning-Based Partial Volume Correction in Standard and Low-Dose PET-CT Imaging," arXiv preprint arXiv:2207.02553, 2022.
[12] M.-S. Azimi, A. Kamali-Asl, M. R. Ay, H. Arabi, and H. Zaidi, "ATB-Net: A novel Attention-based convolutional neural network for predicting full dose from low dose PET images," presented at the 2022 IEEE Nuclear Science Symposium, Medical Imaging Conference and Room Temperature Semiconductor Detector Conference, Japan, 2021.
[13] Arabi H, Zaidi H. Applications of artificial intelligence and deep learning in molecular imaging and radiotherapy. Eur. J. Hybrid Imaging 2020;4(1):1–23.
[14] Arabi H, AkhavanAllaf A, Sanaat A, Shiri I, Zaidi H. The promise of artificial intelligence and deep learning in PET and SPECT imaging (in eng). Phys Med Mar 2021;83:122–37. https://doi.org/10.1016/j.ejmp.2021.03.008.
[15] Sanaat A, Shiri I, Ferdowsi S, Arabi H, Zaidi H. Robust-deep: A method for increasing brain imaging datasets to improve deep learning models' performance and robustness (in eng). J Digit Imaging Jun 2022;35(3):469–81. https://doi.org/10.1007/s10278-021-00536-0.
[16] Islam J, Zhang Y. GAN-based synthetic brain PET image generation (in eng), Brain. Inform Mar 30 2020,;7(1):3. https://doi.org/10.1186/s40708-020-00104-2.
[17] Arabi H, Zeng G, Zheng G, Zaidi H. Novel adversarial semantic structure deep learning for MRI-guided attenuation correction in brain PET/MRI (in eng). Eur J Nucl Med Mol Imaging Dec 2019;46(13):2746–59. https://doi.org/10.1007/s00259-019-04380-x.
[18] Erlandsson K, Wong A, Van Heertum R, Mann JJ, Parsey R. An improved method for voxel-based partial volume correction in PET and SPECT. Neuroimage 2006;31 (Supplement 2):T84.
[19] Thomas BA, Erlandsson K, Modat M, Thurfjell L, Vandenberghe R, Ourselin S, et al. The importance of appropriate partial volume correction for PET quantification in Alzheimer's disease. Eur J Nucl Med Mol Imaging 2011;38(6):1104–19.
[20] Erlandsson K, Buvat I, Pretorius PH, Thomas BA, Hutton BF. A review of partial volume correction techniques for emission tomography and their applications in neurology, cardiology and oncology. Phys Med Biol 2012;57(21):R119.
[21] Xu L, Huang J, Nitanda A, Asaoka R, Yamanishi K. A Novel Global Spatial Attention Mechanism in Convolutional Neural Network for Medical Image Classification, arXiv preprint arXiv:2007.15897, 2020.
[22] Zhang Z, Zhou T, Zhang Y, Pang Y. ttention-based deep residual learning network for entity relation extraction in Chinese EMRs (in eng). BMC Med Inform Decis Mak Apr 9 2019;19(Suppl 2):55. https://doi.org/10.1186/s12911-019-0769-0.
[23] Bahrami A, Karimian A, Fatemizadeh E, Arabi H, Zaidi H. "A new deep convolutional neural network design with efficient learning capability: Application to CT image synthesis from MRI," (in eng). Med Phys Oct 2020;47(10):5158–71. https://doi.org/10.1002/mp.14418.
[24] Bahrami A, Karimian A, Arabi H. Comparison of different deep learning architectures for synthetic CT generation from MR images (in eng). Phys Med Oct 2021;90:99–107. https://doi.org/10.1016/j.ejmp.2021.09.006.
[25] Thomas BA, Cuplov V, Bousse A, Mendes A, Thielemans K, Hutton BF, et al. PETPVC: a toolbox for performing partial volume correction techniques in positron emission tomography. Phys Med Biol 2016;61(22):7975.
[26] Yang J, Huang S, Mega M, Lin K, Toga A, Small G, et al. Investigation of partial volume correction methods for brain FDG PET studies. IEEE Trans Nucl Sci 1996;43(6):3322–7.
[27] Erlandsson K, Buvat I, Pretorius PH, Thomas BA, Hutton BF. "A review of partial volume correction techniques for emission tomography and their applications in neurology, cardiology and oncology," (in eng). Phys Med Biol 2012;57(21):R119–59. https://doi.org/10.1088/0031-9155/57/21/r119.
[28] Fahrig R, et al. Design, performance, and applications of a hybrid X-Ray/MR system for interventional guidance, Proceedings of the IEEE, vol. 96, no. 3, pp. 468-480, 2008.
[29] Gao Y, Zhu Y, Bilgel M, Ashrafinia S, Lu L, Rahmim A. Voxel-based partial volume correction of PET images via subtle MRI guided non-local means regularization. Phys Med 2021;89:129–39.
[30] Arabi H, Zaidi H. "Spatially guided nonlocal mean approach for denoising of PET images," (in eng). Med Phys Apr 2020;47(4):1656–69. https://doi.org/10.1002/mp.14024.
[31] Arabi H, Zaidi H. "Non-local mean denoising using multiple PET reconstructions," (in eng). Ann Nucl Med Feb 2021;35(2):176–86. https://doi.org/10.1007/s12149-020-01550-y.
[32] W.-j. Chen and A. McMillan, "Single subject deep learning-based partial volume correction for PET using simulated data and cycle consistent networks," ed: Soc Nuclear Med, 2020.
[33] Monga V, Li Y, Eldar YC. Algorithm unrolling: Interpretable, efficient deep learning for signal and image processing. IEEE Signal Process Mag 2021;38(2):18–44.